



The microstructure and properties of C and W co-doped NiCr embedded thin film resistors



Li-Fei Lai^{a,b}, Xing-Song Su^b, Xian-Zhu Fu^{b,*}, Rong Sun^{b,*}, Ching-Ping Wong^{c,d}

^a Ningbo University of Technology, Ningbo 315016, PR China

^b Shenzhen Institutes of Advanced Technology, Chinese Academy of Sciences, Shenzhen 518055, PR China

^c Department of Electronics Engineering, The Chinese University of Hong Kong, Hong Kong, PR China

^d School of Materials Science and Engineering, Georgia Institute of Technology, Atlanta, GA 30332-0245, United States

ARTICLE INFO

Article history:

Received 21 July 2014

Accepted in revised form 19 September 2014

Available online 28 September 2014

Keywords:

C and W co-doped NiCr alloy

Embedded resistor

Microstructure

Electrical properties

Corrosion resistance

ABSTRACT

C and W co-doped NiCr alloy flexible thin films were prepared using closed magnetic field unbalanced magnetron sputtering method on a copper foil substrate. The microstructure, electrical properties, and corrosion resistance of the co-doped NiCr thin film were investigated and analyzed as embedded resistor materials. After co-doping, the alloy thin film embedded resistor materials exhibited considerably lower temperature coefficient of resistance (TCR), larger sheet resistance and higher corrosion resistance comparing to the NiCr alloy thin film embedded resistor materials.

© 2014 Elsevier B.V. All rights reserved.

1. Introduction

With the miniaturization of electronic products, conventional discrete passive components are reaching their physical limit on the printed circuit board (PCB). Comparing to the traditional discrete passive components, thin film embedded passive components have many advantages such as small surface space, low electromagnetic interference and installation cost, high performance and signal quality by reducing the wiring distance and the number of solder joints, etc [1,2]. Resistor is one of the very usually used passive components [3]. In recent years, thin film embedded resistors [TFER] have attracted increasing research on different materials, such as NiCr [1,4], NiP [2,5], CrSi [6], TiW [7] and TaN [8–10]. Among the materials, NiCr based alloys have been especially intensively developed as promising TFERs since they possess high electrical resistivity and good reliability [1,11–17]. However, there are still more high requirements for NiCr alloy as thin film embedded resistors, for example: larger sheet resistance, lower temperature coefficient of resistance (TCR), higher corrosion resistance, etc.

Herein, we report C and W co-doped NiCr alloy thin films fabricated by magnetron sputtering method as high performance TFER materials. The microstructure and properties of the co-doped NiCr TFER were also investigated.

2. Experimental

The C and W co-doped NiCr thin films were deposited by closed-field unbalanced magnetron sputtering ion plating (CFUMSIP) as a versatile technique for the preparation of high-quality coatings. NiCr (80/20 at.%) alloy (99.99% purity), C (99.99% purity) and W (99.99% purity) were used as target for the sputtering. High purity Ar (99.999% purity) was introduced as the sputtering gases. The argon pressure was 1.2×10^{-3} Torr, the substrate temperature was 27 °C, the gas flow of 25 sccm, the base pressure of chamber was 4.0×10^{-5} Torr, and the rotation speed was 4 rpm. The sputtered time was set at 4 min. To achieve good adhesion and large sheet resistance, the C and W co-doped NiCr thin films were deposited on the matte side of electrolytic copper foil with very low profile (VLP). Based on the preparing optimizational preparation experimental, C and W co-doped NiCr thin films were performed under the sputtering conditions: bias voltage was 90 V, NiCr target current was 3 A, C target current was 1 A, and W target current was 0.1 A. The thin films were annealed with RTP500 (Rapid Thermal Processor, Beijing Institute of Applied Physics, China) in N₂ for 540 s at 250 °C, 300 °C, 350 °C, 400 °C and 500 °C, respectively.

The surface morphology of thin film embedded resistor materials was examined by SEM (Hitachi S-4800) and AFM (CSPM5000). The phase structures of thin film embedded resistors were analyzed by XRD (X'pert PRO, NL). The surface chemical state of thin film embedded resistor materials was investigated by XPS (ULVAC-PHI 1800) using a 1486.6 eV Al $k\alpha$ source. All binding energy values were compensated

* Corresponding authors. Tel.: +86 755 86392151; fax: +86 755 86392299.
E-mail addresses: lailf-325@163.com (L.-F. Lai), xz.fu@siat.ac.cn (X.-Z. Fu), rong.sun@siat.ac.cn (R. Sun).

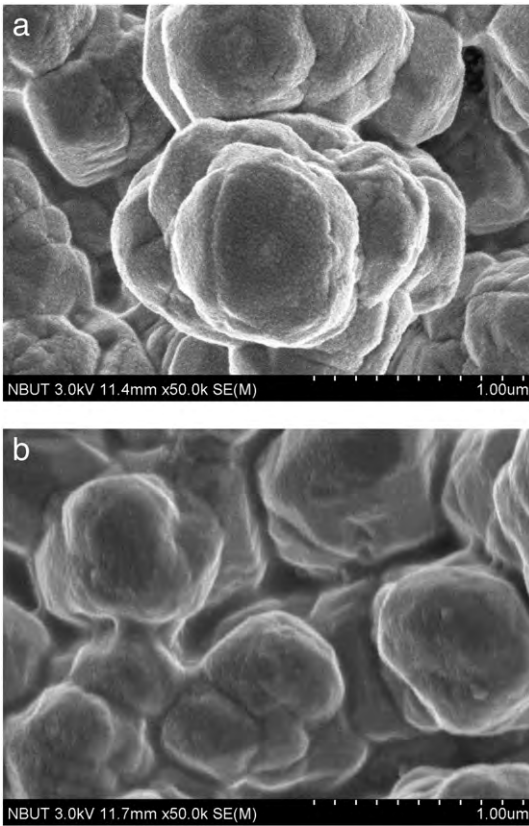


Fig. 1. SEM surface images of different thin films in as-deposited states: (a) C/W co-doped NiCr; (b) NiCr.

to C1s (284.5 eV); the sputter rate is 8.0 nm min^{-1} for depth profiling by SiO_2 as the scale of standard sample and argon gas as the sputtering gas. The carbon in C and W co-doped NiCr thin films was analyzed by Raman spectroscopy (Renishaw inVia). The thickness of NiCr alloy on the top of copper foil was determined by the alloy thickness on the top of float glass by a calibrated surface profiler (Model XP-1) since the copper foil was too soft [13]. The corrosion resistances were measured by using polarization curves with an electrochemical workstation (Zennium, Zhaner Elektrik, Germany).

In order to analyze the thermal stability, the TFER were rapidly heated to $250 \text{ }^\circ\text{C}$ at a rate of $40 \text{ }^\circ\text{C/min}$, then gradually cooled down at a rate of $20 \text{ }^\circ\text{C/min}$ by the detection probing station (HFSE-PB4). The sheet resistance of thin film embedded resistor was measured using a digital source meter (Keithley 2410) with the step of $10 \text{ }^\circ\text{C}$ in the cooling process. The TCR is defined as $TCR = \frac{(R_t - R_{t_0})}{R_{t_0} (t - t_0)} \times 10^6 \text{ (ppm/K)}$, where R_{t_0} and R_t are the sheet resistance of thin film embedded resistor measured at the temperature of t_0 (room temperature) and t , respectively.

3. Results and discussion

3.1. Surface morphology

Fig. 1 showed the SEM images of the NiCr and C/W co-doped NiCr thin films in as-deposited states. It could be found that the surface morphology of C/W co-doped NiCr thin film was clear, and the particles on the surface were large and tight, while that of NiCr thin film was unclear; some places such as filaments were connected into the network structure. The SEM image showing the morphology of C/W co-doped NiCr thin films was clearer than that of NiCr thin film. This might result from an increase in the electrical conductivity of the C/W co-doped film surface. In addition, the presence of some oxides in the NiCr thin film might cause a low conductive area on the surfaces of the thin film. Fig. 2 displayed the three-dimensional AFM images of NiCr and C/W

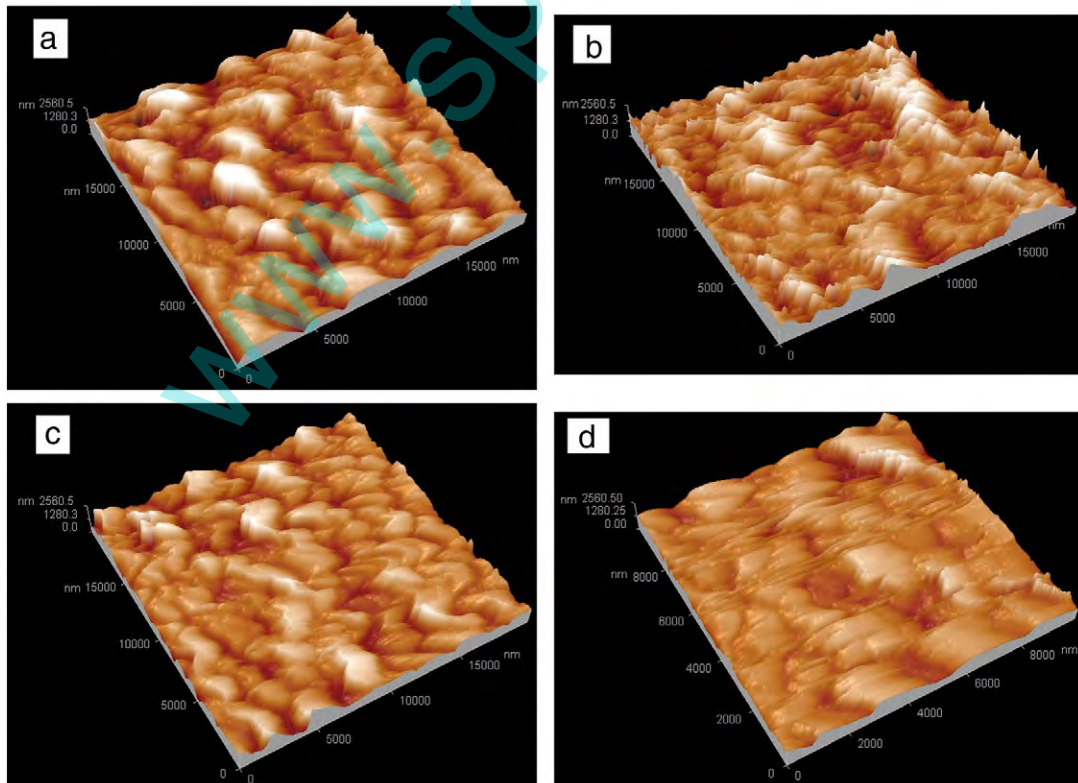


Fig. 2. AFM 3D images of different thin films before and after annealed at $300 \text{ }^\circ\text{C}$: (a) (c) C/W co-doped NiCr; (b) (d) NiCr.

co-doped NiCr thin films before and after annealed at 300 °C in a scanning area of 20 $\mu\text{m} \times 20 \mu\text{m}$. The C/W co-doped NiCr thin film surface had lower roughness, larger particles and fewer defects than that of the NiCr thin film in as-deposited state (Fig. 2(a) (b)). Carbon has a smaller radius than Ni and Cr, so it might penetrate into the pores and defects in the C/W co-doped NiCr thin film and form a more compact arrangement of atoms under suitable conditions. The case might not happen for W atom since its radius is larger than that of Ni and Cr atoms. But small amounts of W doping were not enough to affect the film morphology. As shown in Fig. 2(c) and (d), the particles on the thin film surface became dense, and the defects in C/W co-doped NiCr and NiCr thin films were reduced when they were annealed at 300 °C. But the surface morphology of them was different; the particles on the C/W co-doped NiCr thin film surface were more uniform. Thus, C and W co-doping could reduce the defects and holes in the NiCr thin films and improve the resistance stability of NiCr thin films.

3.2. Phase structure

Fig. 3 showed the XRD patterns of NiCr and C/W co-doped NiCr thin films before and after annealed at 300 °C. Only a diffraction peak appeared in the two thin films in as-deposited state, respectively. The hexagonal structure of Ni (011) appeared in the NiCr thin film, while the face-centered structure of Ni (111) appeared in the C/W co-doped NiCr thin film. These phase structures were attributed to the differences

in the kinetic energy of Ni atoms impinging on the substrates [18]. The co-sputtered C and W atoms might have an effect on the kinetic energy of the deposited nickel atoms and caused the Ni (111) to have minimum surface energy or strain energy, leading to a preferred orientation. Thus the nickel crystals transformed to the usual face-centered structure from the hexagonal structure. The different crystal structure would affect the resistance stability of thin films [19], so the Ni (111) appearing in the C/W co-doped NiCr thin film might improve the electrical properties of the C/W co-doped NiCr thin film. After annealed at 300 °C, the weak Ni (200) peak was observed in the C/W co-doped NiCr thin film, and the Ni (010), Ni (002), Ni (011), Cr (110) and Cr (200) appeared in the NiCr thin films. The broad diffraction peaks indicated that these thin films were not fully crystallized. The diffraction peaks of the NiCr thin film seemed to be stronger than that of the C/W co-doped NiCr thin film, suggesting the better crystalline of the NiCr thin film. Cr diffraction peaks did not appear in Fig. 3(a); this reason could be interpreted by the NiCr phase diagram. There is mainly a Ni single phase solid solution, and most of the Cr element dissolves in the Ni crystal lattice as a metallic element as the Cr concentration is 20 at.%; the temperature is lower than 1200 °C [20]. The diffraction peaks of C and W in the C/W co-doped NiCr thin film were not found since carbon mainly existed in the amorphous form and tungsten content was less than 2 wt.%.

3.3. Composition

Fig. 4(a) showed the full XPS spectra of the C/W co-doped NiCr thin film before and after annealed at 300 °C, 400 °C and 500 °C,

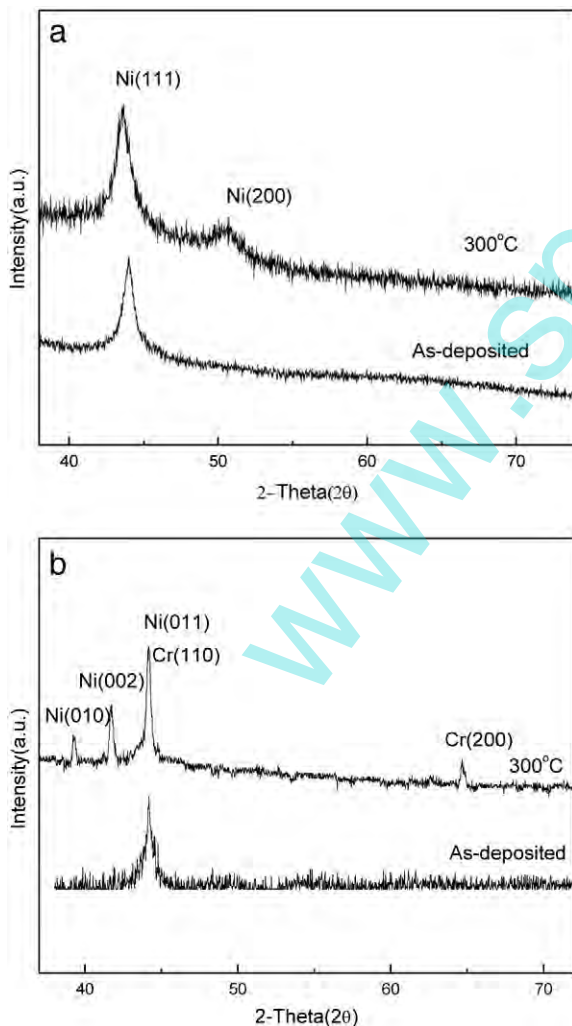


Fig. 3. XRD patterns of different thin films before and after annealed at 300 °C: (a) C/W co-doped NiCr; (b) NiCr.

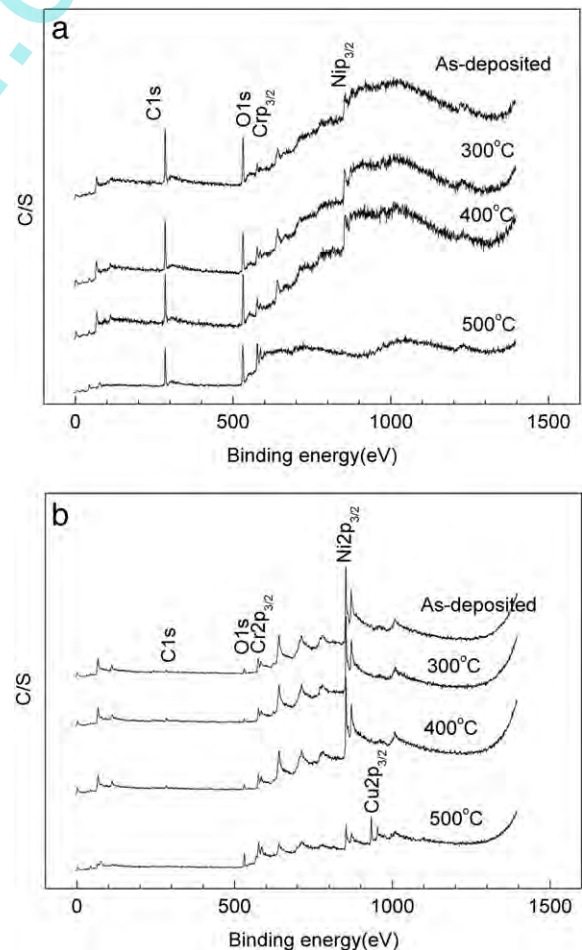


Fig. 4. XPS spectra obtained from the C/W co-doped NiCr thin film: (a) on surface; (b) after 75 s of sputtering.

respectively. The surface content of Ni element which is determined from XPS results decreased with the annealing temperature rising. There was no Ni element observed on the surface after annealing at 500 °C. On the contrary, the surface content of Cr element increased with the annealing temperature increasing because Cr was easily oxidized and would segregate toward the surface at high temperature annealing [13]. The surface content of O element had little change after annealing at 400 °C and 500 °C. It might be that the Cr-oxides covering on the surface of thin films hindered the further oxidation of the thin films. The content of C element was always high on the surface of the thin film in different annealing temperatures, which might be resulted from the contaminant in the XPS test. Fig. 4(b) showed the full XPS spectra of C/W co-doped NiCr thin film after sputtering the thin film surface for 75 s. It was found that the contents of Cr and O elements increased while the contents of C and Ni elements decreased with the annealing temperature increasing. But there was rarely C after annealing at 500 °C. The Cu element appeared on the surface after annealing at 500 °C, indicating that the Cu atoms in the substrates had diffused into the C/W co-doped NiCr thin film at high annealing temperature. The diffusion rate of Cu atoms increased with the temperature increasing; thus Cu atoms penetrated through the interface into the C/W co-doped NiCr thin film at high annealing temperature. The segregation and diffusion of the metal atoms in the C/W co-doped NiCr thin film could affect its electrical properties [21]. The W element had not been found on the surface of the thin film because the W content was poor and the surface of the thin film was mainly covered by Cr-oxides.

Fig. 5 showed the narrow scan spectra of Ni2p3/2 on the surface of C/W co-doped NiCr thin films before and after annealing. Ni metal was detected at binding energies of 852.42 eV as the predominant Ni state. Small amounts of NiO (855.02 eV) and Ni₂O₃ (855.80 eV) were also detected as shown in the fitted Gaussian curves. The XPS area ratios of the chemical states of Ni species for the C/W co-doped NiCr thin film before and after annealing were presented in the Table 1. Ni metal decreased and Ni-oxides had little change with the temperature increasing. It might be that Cr was easy to generate the dense Cr-oxides covering on the surface of thin film and prevented Ni from further oxidation. The surface of the C/W co-doped NiCr thin film was completely occupied by Cr-oxides when annealed at 500 °C; thus Ni was not observed on the surface.

Fig. 6 presented the narrow scan spectra of Cr2p3/2 on the surface of the C/W co-doped NiCr thin film before and after annealing. The XPS area ratios of the chemical states of Cr species before and after annealing were presented in Table 2. Cr³⁺ as the predominant Cr state was detected at the binding energy of 576.6 eV and as complete Cr state presented after annealing at 500 °C, indicating that Cr was easily oxidized at high temperature.

Fig. 7 showed the XPS spectra peaks of C1s before and after annealing at 500 °C, the peaks at 284.4 eV and 285.4 eV were assigned to sp² and sp³, respectively. The XPS area ratios of sp² and sp³ in as-deposited state were 87.10% and 12.90%, respectively; when annealed at 500 °C, they were 84.37% and 15.63%, respectively, which embodied the characteristics of amorphous carbon. The amount of sp³-bonded carbon in thin films increased with annealing temperature increasing. The increasing sp³ bonding may raise stress of the amorphous carbon film, which would affect the electrical properties of the films [22,23], so the C/W co-doped NiCr thin film in Fig. 11(b) annealed at high temperatures did not exhibit a low TCR. The sp² was mainly the hybridized state of C1s, indicating that the carbon mainly existed as a graphite-like structure.

Table 3 showed the EDS analysis of the C/W co-doped NiCr thin film under different annealing temperatures. EDS could detect elements much deep in the samples than XPS method. It could be found that the atomic ratios of Ni and Cr in thin film were close to 20/80 at.%, and were almost the same with the target. The increasing of Cr on the surface of the thin film with the annealing temperature rising in Fig. 4(a) actually resulted from the segregation of Cr at high annealing

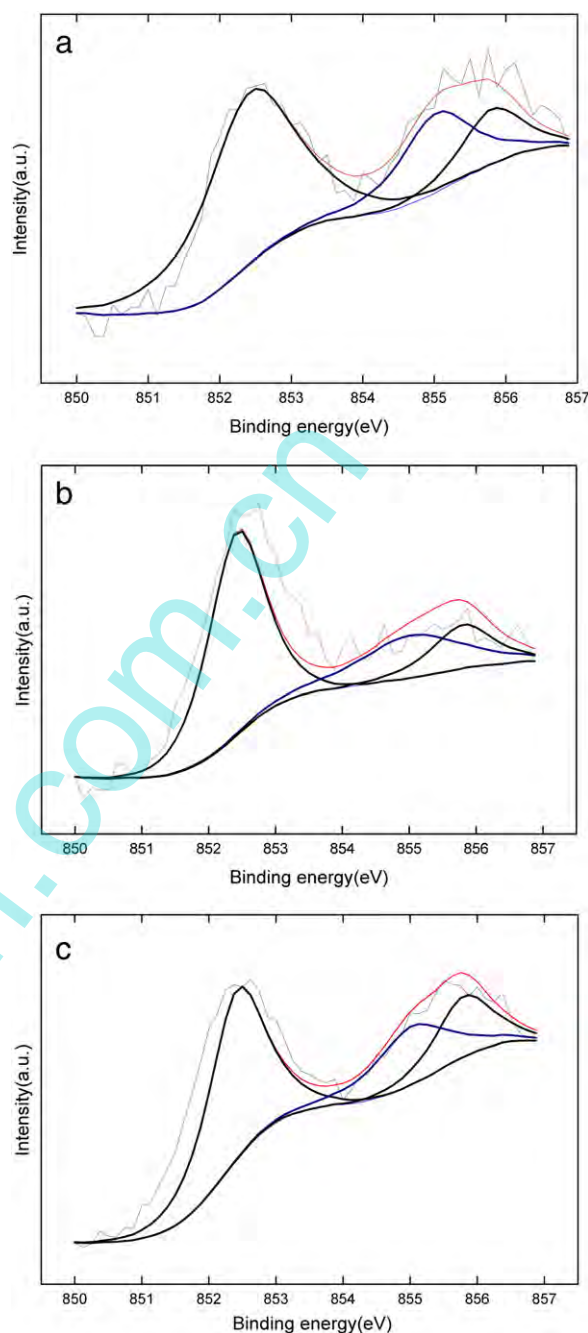


Fig. 5. XPS spectra of Ni obtained from the C/W co-doped NiCr thin film surface before and after annealing: (a) as-deposited state; (b) 300 °C; (c) 400 °C.

temperature. The Cu content was the highest in Table 3, which derived from the copper substrate, because the film thickness was less than 200 nm and the detection depth of EDS would be more than one micron. The W and C element in thin film existed as a single substance because

Table 1
XPS area ratios of chemical states of Ni species for the C/W co-doped NiCr thin film before and after annealing.

BE (eV)	XPS area ratio (%)				
	As-deposited	300 °C	400 °C	500 °C	
Ni	852.42	63.09	61.11	55.37	0
Ni ²⁺	855.02	23.27	23.96	24.77	0
Ni ³⁺	855.80	13.64	14.93	19.86	0

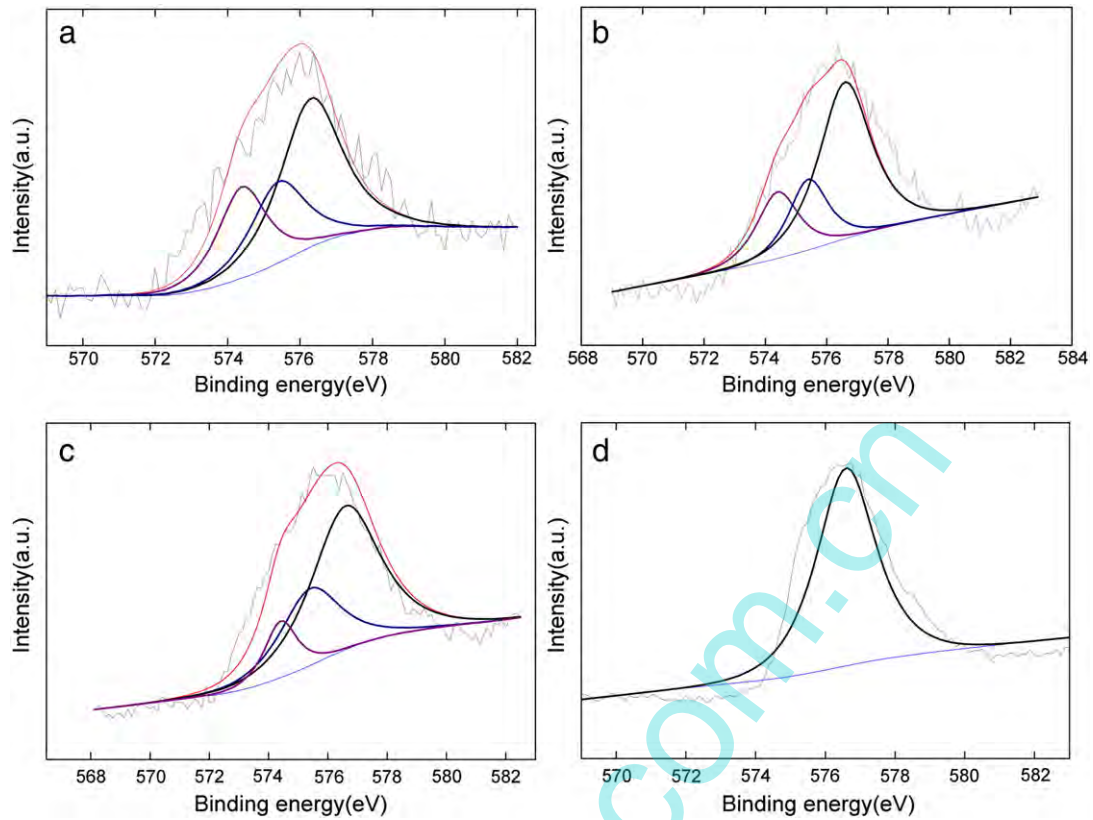


Fig. 6. XPS spectra of Cr obtained from the C/W co-doped NiCr thin film surface before and after annealing: (a) as-deposited state; (b) 300 °C; (c) 400 °C; (d) 500 °C.

they were hard to be oxidized at annealing in the range of 300 °C–500 °C.

3.4. Raman analysis

Since C might mainly keep its amorphous structure and its content was less in the C/W co-doped NiCr thin films, it was very difficult to be detected by XRD technique. Raman spectroscopy is a powerful tool to fully characterize disorder in graphite and is an effective means for analyzing C microcrystal. As shown in Fig. 8, the C Raman peak appeared until the annealing temperature increased to 400 °C. The 'D' located at 1355.39 cm^{-1} , 'G' at 1586.60 and 1593.95 cm^{-1} , 'G' at 2727.32 and 2709.97 cm^{-1} appeared for the C/W co-doped NiCr thin film annealed at 400 °C and 500 °C, respectively. The higher the annealing temperature, the greater the intensity of the Raman peaks. The G peak is due to the bond stretching of all pairs of sp^2 atoms in both rings and chains. The G band corresponds to the symmetric E_{2g} vibrational mode in graphite-like materials. The D peak is due to the breathing modes of sp^2 atoms in rings, and is caused by A_{1g} non-active vibrations mode [24]. G' for the second-peak of G is related to graphite transverse optical phonon branches [25]. In addition, the weak scattering peaks appeared

at 500 cm^{-1} and 700 cm^{-1} , which was mainly induced disorder scattering [26]. The half-height peak width decreased with annealing temperature increasing in Fig. 8, indicating that the crystallization of C increased, phonon lifetime with correspond extended, and the width of line with correspond narrowed [27]. The D and G peaks were fitted with Lorentzian by fitting the data in Table 4. The $R = I_D/I_G$ can reflect the degree of carbon graphitization: C has high graphitization and good microcrystalline orderliness when R is the small. Thus the microcrystalline of C was better when the film was annealed at 500 °C than that of the film annealed at 400 °C. Because the annealing treatment can reduce the concentration of sp^2 carbon clusters [28]. The degree of carbon graphitization of the thin films increases, the electrical resistivity of thin films might decrease [29], so C/W co-doped NiCr thin films need not be annealed at high temperature.

3.5. Electrical properties

Fig. 9 showed the temperature dependence of TCR of NiCr, C and W co-doped NiCr thin films in as-deposited states. Comparing to the NiCr thin film, the TCR absolute value of the C/W co-doped NiCr thin film was smaller, especially in the testing temperature range from room temperature to 250 °C. In addition, the TCR–T curve of the C/W co-doped NiCr thin film was also more stable than that of the NiCr thin film. The results suggested that the C/W co-doped NiCr thin film embedded resistors had more resistance stability than NiCr thin film embedded resistors when they were working in the electrics. As shown in Fig. 10, the C/W co-doped NiCr thin film embedded resistors in as-deposited states showed larger sheet resistance than the NiCr thin film embedded resistors which was beneficial for its application. The doped carbon in the NiCr thin film could cause the increasing disordered atomic arrangement and big sheet resistor [30]. In addition, W doping might improve the resistivity of the NiCr thin film due to the larger resistivity of W metal.

Table 2

XPS area ratios of chemical states of Cr species for the C/W co-doped NiCr thin film before and after annealing.

BE (eV)	XPS area ratio (%)				
	As-deposited	300 °C	400 °C	500 °C	
Cr	574.4	24.76	20.23	11.40	0
Cr ²⁺	575.4	24.83	20.20	28.55	0
Cr ³⁺	576.6	50.41	59.58	60.0	100

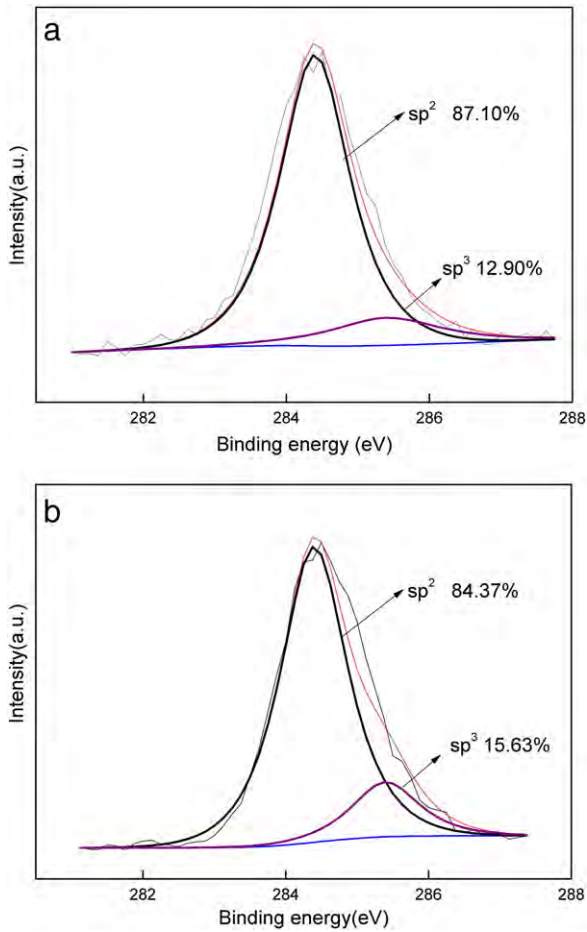


Fig. 7. The peak fitting C1s XPS spectra in the C/W co-doped NiCr thin film: (a) as-deposited state; (b) 500 °C.

Fig. 11(a) and (b) showed the temperature dependence of TCR of the C/W co-doped NiCr and NiCr thin film before and after annealing at 250, 300 °C, 350 °C, 400 °C, and 500 °C, respectively. The smallest fluctuation in TCR of NiCr and C/W co-doped NiCr thin films was obtained when the annealing temperature was 300 °C since most of the residual stress of thin films might be eliminated at this temperature. The TCR values had a large fluctuation when the thin films were annealed at 350 °C, 400 °C and 500 °C. The defects and stress of thin films could not be sufficiently eliminated if the rapid thermal annealing was only 540 s because the surface of the thin film had been oxidized [19]. In addition, the high annealing temperature strengthened metal segregation and diffusion, which might change the inner stress and affect the electrical properties of thin films. The TCR absolute value of the C/W co-doped NiCr thin film annealed at 300 °C was in the range of 2.86–199.97 ppm/K, which were much smaller than those

Table 3
Element concentrations analyzed by EDS in the C/W co-doped NiCr thin film before and after annealing.

	As-deposited	300 °C	400 °C	500 °C
Ni (at.%)	10.57	7.78	8.54	7.10
Cr (at.%)	2.27	1.62	2.20	2.19
C (at.%)	0	20.98	17.87	18.30
W (at.%)	0	0.07	0.14	0.14
O (at.%)	4.36	2.90	3.20	5.06
Cu (at.%)	82.80	66.64	68.04	67.21
Ni:Cr	4.66	4.80	3.88	3.24

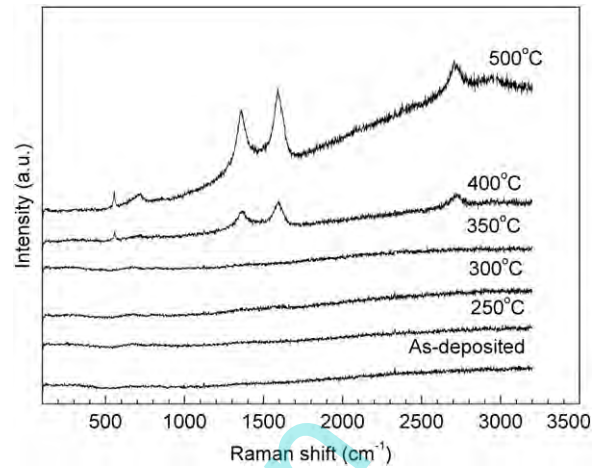


Fig. 8. Raman spectra of C in the C/W co-doped NiCr thin film at different annealing temperatures.

of the NiCr film in the range of 35.26–327.31 ppm/K. The C/W co-doped NiCr thin film was mostly negative in the range of 54.29–244.02 ppm/K, and the TCR of NiCr were all positive in the range of 80.71–567.15 ppm/K in as-deposited state. Thus C and W co-doping could reduce the TCR and improve the electrical properties of the NiCr thin film.

3.6. Corrosion resistance

Fig. 12 showed the polarization curves of NiCr and C/W co-doped NiCr thin film in as-deposited state and annealing at 300 °C. The corrosion currents of C/W co-doped NiCr thin films were always smaller than that of the NiCr thin film. The corrosion potential of the C/W co-doped NiCr thin film was higher than that of the NiCr thin film in as-

Table 4

The parameters of the C Raman spectra in the C/W co-doped NiCr thin film in different annealing temperatures.

Anneal. tem.	W (D)/cm ⁻¹	W (G)/cm ⁻¹	H _D /a.u.	H _G /a.u.	R (I _D /I _G)	FWHM (D)/cm ⁻¹	FWHM (G)/cm ⁻¹
400 °C	1355.39	1586.60	170.48	265.96	0.641	80.26	72.17
500 °C	1355.39	1593.95	499.22	789.92	0.632	57.58	70.58

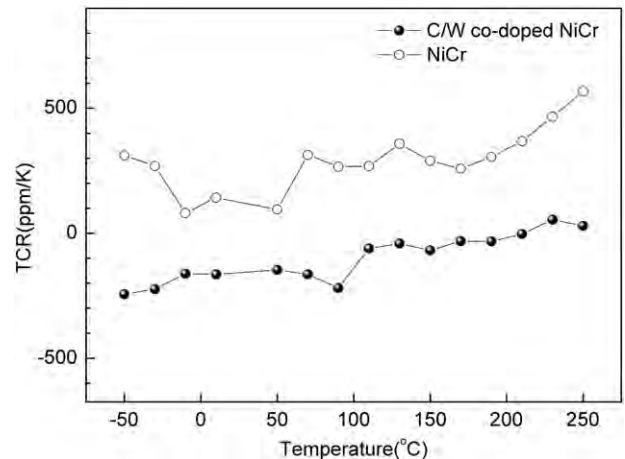


Fig. 9. The temperature dependence of the TCR of NiCr and C/W co-doped NiCr thin film in as-deposited states.

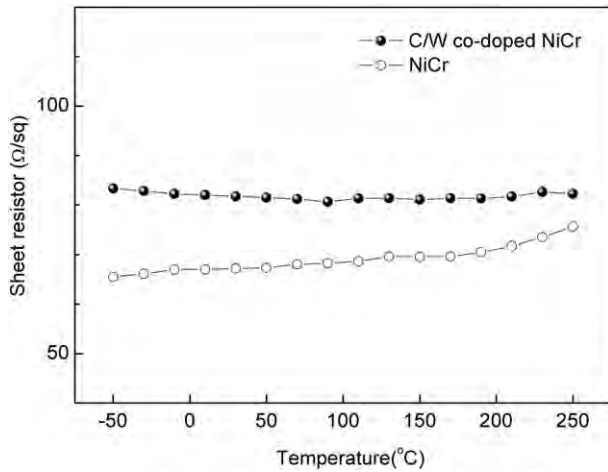


Fig. 10. The temperature dependence of the sheet resistor of NiCr and C/W co-doped NiCr thin film in as-deposited states.

deposited state. The results indicated that C and W doping in the NiCr thin film could help to increase the corrosion resistance of the films. Because carbon in the C/W co-doped NiCr thin film mainly existed in the form of an amorphous and microcrystalline hybrid structure. Their hybrid interface might improve the diffusion of Cr; thus Cr was easier to generate a dense chromium oxide layer on the surface of thin films.

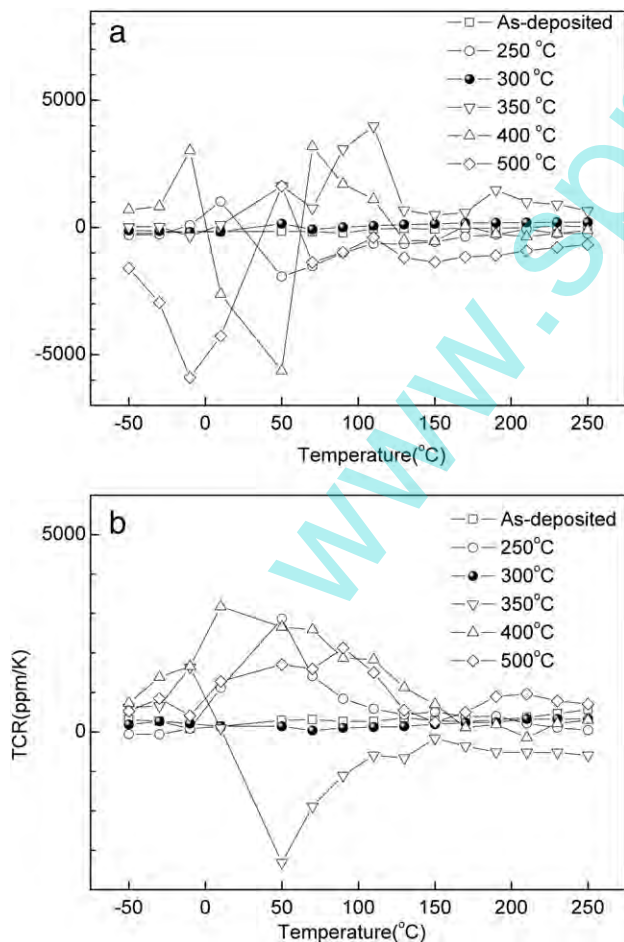


Fig. 11. The temperature dependence of the TCR of thin films under different annealing temperatures: (a) C/W co-doped NiCr; (b) NiCr.

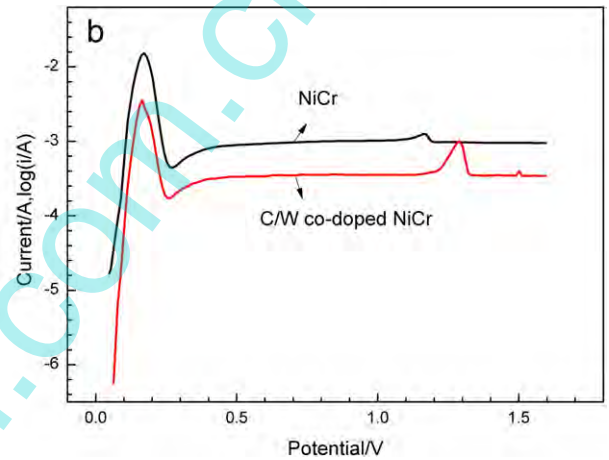
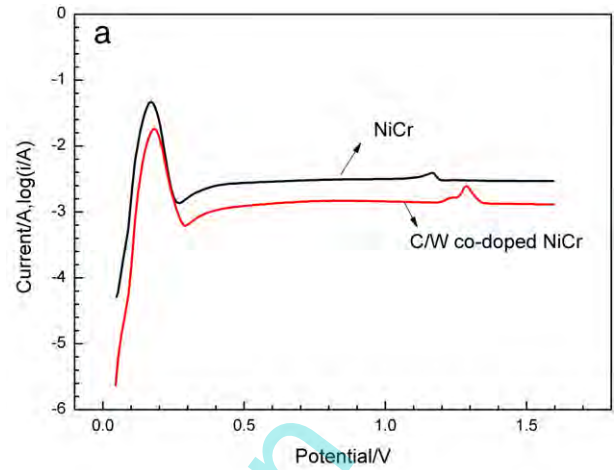


Fig. 12. Comparison of corrosion resistance of the C/W co-doped NiCr and NiCr thin film before and after annealing: (a) as-deposited state; (b) 300 °C.

W metal is very stable; it will not react with hydrochloric acid and sulfuric acid, and does not dissolve in king water.

C/W co-doped NiCr and NiCr thin films in as-deposited states were soaked in 60% H_2SO_4 for 85 h. Their SEM images after corroded were shown in Fig. 13. The C/W co-doped NiCr thin film was only partially destroyed, and some particles were connected into small pieces. Some parts of the NiCr thin film were eroded into small particle agglomeration, and the small part became blocky. Therefore C and W co-doping could improve the corrosion resistance of NiCr thin films.

4. Conclusions

The studied NiCr thin film co-doped with C and W elements by closed magnetic field unbalanced magnetron sputtering method revealed a new C/W co-doped NiCr thin film embedded resistor material. The C/W co-doped NiCr thin film demonstrated more stable electrical performance, larger sheet resistor and good corrosion resistance than NiCr thin film. The TCR absolute value of the C/W co-doped NiCr thin film before and after annealing at 300 °C was in the range of 54.29–244.02 ppm/K and 2.86–199.97 ppm/K, respectively. The TCR of NiCr was in the range of 80.71–567.15 ppm/K and 35.26–327.31 ppm/K, respectively. The preferred orientations of the C/W co-doped NiCr thin film was Ni (111), while that in the NiCr thin film was Ni (011). The different crystal orientations would influence the electrical properties of the thin film. Carbon with an amorphous structure mainly in deposited C/W co-doped NiCr thin film might decrease the defects and improve the electrical properties and corrosion resistance of the thin film.

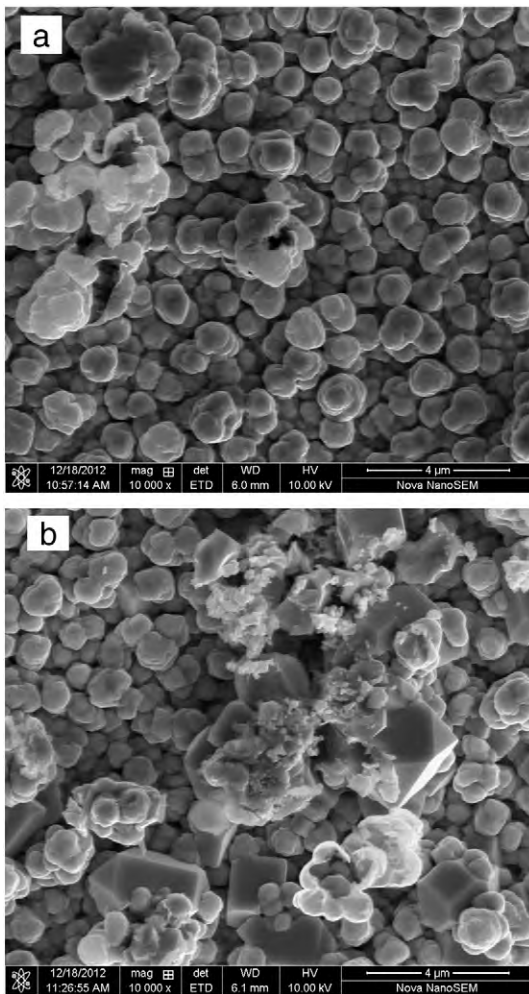


Fig. 13. SEM surface images of the C/W co-doped NiCr and NiCr thin film corroded in as-deposited state: (a) C/W co-doped NiCr; (b) NiCr.

W with large resistivity and stable chemical properties might enhance the sheet resistor and corrosion resistance of the C/W co-doped NiCr thin film.

Acknowledgments

This work was financially supported by the National Natural Science Foundation of China (no. 21203236), Guangdong and Shenzhen Innovative Research Team Program (nos. 2011D052, KYPT20121228160843692), the Shenzhen Electronic Packaging Materials Engineering Laboratory (2012-372), the Scientific Research Fund of the Zhejiang Provincial Education Department (Y201326895), and the Ningbo Natural Science Foundation (2014A610153).

References

- [1] J. Wang, R. Hilburn, S. Clouser, B. Greenlee, Proceedings of the IPC Annual Meeting, Louisiana, U.S.A, November 2002, pp. S03–S04.
- [2] G. Min, Synth. Met. 153 (2005) 49–52.
- [3] H.F. Lee, C.Y. Chan, C.S. Tang, J. Mater. Process. Technol. 207 (2008) 72–88.
- [4] M. Oppermann, MCM '94 Proceedings, Denver, April 1994, pp. 279–284.
- [5] G.y. Zhou, W. He, S.x. Wang, C.y. Chen, C.P. Wong, Mater. Lett. 108 (2013) 75–78.
- [6] T. Lenihan, L. Schaper, Y. Shi, G. Morcan, J. Parkerson, Proceedings of the IEEE 46th Electronic Components and Technology Conference, Orlando, May 1996, pp. 119–124.
- [7] D. Scheid, MCM '94 Proceedings, Denver, April 1994, pp. 273–278.
- [8] I.S. Park, S.Y. Park, G.H. Jeong, S.J. Suh, Thin Solid Films 516 (2008) 5409–5413.
- [9] S.M. Kang, S.G. Yoon, S.J. Suh, D.H. Yoon, Thin Solid Films 516 (2008) 3568–3571.
- [10] K.L. Coates, C.P. Chien, Y.R. Hsiao, et al., Proceedings of the 1998 International Symposium on Microelectronics, San Diego, November 1998, pp. 490–495.
- [11] L.F. Lai, X.Z. Fu, R. Sun, R.X. Du, Surf. Coat. Technol. 235 (2013) 552–560.
- [12] L.F. Lai, W.J. Zeng, X.Z. Fu, R. Sun, R.X. Du, Surf. Coat. Technol. 218 (2013) 80–86.
- [13] L.F. Lai, W.J. Zeng, X.Z. Fu, R. Sun, R.X. Du, J. Alloys Compd. 538 (2012) 125–130.
- [14] I.H. Kazi, P.M. Wild, T.N. Moore, M. Sayer, Thin Solid Films 433 (2003) 337–343.
- [15] M.F. Morks, C.C. Berndt, Appl. Surf. Sci. 256 (2010) 4322–4327.
- [16] M. Danişman, N. Cansever, J. Alloys Compd. 493 (2010) 649–653.
- [17] D. Chrisey, J. Fitz-Gerald, R. Auyeung, et al., Appl. Surf. Sci. 154–155 (2000) 593–600.
- [18] P. Pouloupoulos, V. Kapaklis, C. Politis, P. Schweiss, D. Fuchs, J. Nanosci. Nanotechnol. 6 (4) (2006) 3867–3870.
- [19] J.W. Yan, J.C. Zhou, Int. J. Mod. Phys. B 21 (2007) 4561–4574.
- [20] S. Vinayak, H.P. Vyas, K. Muraleedharan, et al., Thin Solid Films 514 (2006) 52–57.
- [21] W. Brückner, J. Schumann, S. Baunack, et al., Thin Solid Films 258 (1995) 236–246.
- [22] P. Fallon, V. Veerasmay, C. Davis, et al., Phys. Rev. B 48 (1993) 4777–4782.
- [23] S. Chowdhury, M.T. Laugier, I.Z. Rahman, et al., Thin Solid Films 447–448 (2004) 174–180.
- [24] X.Y. Lin, K.L. Zhang, K. Hu, et al., ECS Trans. 34 (2011) 793–797.
- [25] A. Cuesta, P. Dhamelincourt, J. Laureyns, Carbon 32 (1994) 1523–1532.
- [26] W.S. Bacsá, J.S. Lannin, D.L. Pappas, et al., Phys. Rev. B 47 (1993) 10931–10934.
- [27] G.X. Cheng, Raman and Brillouin Scattering—Principle and Application, Science Press, Beijing, 2001.
- [28] H. Huang, Z.W. Deng, D.C. Li, et al., Semicond. Sci. Technol. 25 (2010) 045023.
- [29] Y.H. Lin, H.D. Lin, C.K. Liu, et al., Thin Solid Films 518 (2009) 1503–1507.
- [30] M.A. Howson, J. Phys. F Met. Phys. 14 (1984) L25–L31.